IOSUD - Universitatea Politehnica Timişoara
Şcoala Doctorală de Studii Inginereşti

Dezvoltarea, optimizarea și caracterizarea unor straturi de NiCrBSi-TiB_2 pulverizate termic cu flacără și retopite în cuptorul cu vid

Development, optimization and characterization of NiCrBSi-TiB_2 vacuum fused flame-sprayed coatings

Teză de doctorat – Rezumat în limba engleză

pentru obținerea titlului științific de doctor la

Universitatea Politehnica Timișoara

în domeniul de doctorat Ingineria Materialelor

autor ing. Norbert Kazamer

conducător științific Prof.univ.dr.ing. Viorel-Aurel Șerban

luna iunie anul 2019

Contents

1. Motivation

The coating deposition technology developed to a point where it can be used almost on any material, benefiting a large variety of economical branches [1]. Metals, oxides, cermets gradient depositions, reinforcements and in situ synthesis are all used to create different coatings for industries like automotive, chemical processing, mills, aerospace, food processing, oil and gas exploration, medical, nuclear, textile or transportation [2]. Materials have enormously progressed for outstanding functional performances, however, a high demand still exists for protection in different harmful environments.

The life of the component can be extended through several means. An important part of them are directed towards reducing the adhesive, abrasive, erosive wear or lower the corrosion realized through exposure to different environments. Functional performances like high temperature exposure or reconditioning of coatings can guide for a more performant field.

After the production of the coating, the article in its life cycle is greatly challenged by degradation very likely caused by wear and corrosion. Even though the expertise of the researchers and industry greatly increased during the last decades, they are constantly confronted to damage turning to unwanted expenditures. The cost of both wear and corrosion is believed to be a significant fraction of the national GDP's of about 3-5% and reaching in the developing countries even up to 10% [3,4]. Thermal sprayed coatings among other important techniques like inhibitors or cathodic protection contribute in protecting from damages.

2. Aim of the work

Taking into account the present state of art in the direction of wear and corrosion resistant coatings and considering the demand of the market with regard to optimization and post-treatment, the topic of the current research is focusing on investigating the characteristics of flame sprayed and post-treated coatings using as feedstock NiCrBSi, one of the most established Ni-based powders, reinforced with TiB_2 particles.

The chosen reinforcement powder used for this work is TiB_2, a ceramic material known for its high melting point, low density and good hardness. NiCrBSi and TiB_2 have common elements in their chemical composition, and through mechanical mixing, deposition and through an optimized and well-chosen post-treatment performant coatings can be obtained. A post-treatment increases the probability to create a metallurgical bonding and in consequence a strong adhesion to the substrate. A statistical approach was used to optimize the holding time and temperature during the vacuum furnace heat treatment and to select the best proportions among the samples with different matrix-reinforcement volumetric concentration. Possible applications of the gathered results are ones where ductile, corrosion and wear resistant parts are needed like heat exchangers, turbine, extruders, laminators or the agriculture industry.

3. Methodology

The matrix and the reinforcement have been mixed in four different volumetric proportions using a screw conveyer. After the deposition process of the material on a low-alloyed steel, to maximize the results, an optimization through design of experiments was performed to the matrix-reinforcement fraction on one side and to three response variables (porosity, hardness and standard deviation of the hardness) through the variation of two of the most important heat-treatment parameters, time and temperature, on the other one. Thermal behaviour of the selected powder was analysed with the aid of the Differential Thermal Analysis (DTA). Light and confocal scanning laser microscopy (CSLM) were employed for image processing, microstructure and wear track analysis. The morphology, chemical composition as well as the quality of the coating-substrate interface region have been examined using Scanning Electron Microscopy (SEM) combined with Energy Dispersive Spectroscopy (EDX). For the determination of the phase changes during the heat treatment, the powder, the as-sprayed and the heat-treated coating were analysed using X-Ray Diffraction (XRD). The size and distribution of pores have been processed using image analysis. Surface and cross-section hardness was evaluated by Vickers indentation. Tribological investigation using a pin-on-disc arrangement helped compare the friction coefficient and calculate the wear rates of the post-processed samples with another reference sample. Electrochemical corrosion tests were employed to evaluate the corrosion behaviour the developed coating and a reference sample using potentiodynamic polarization with a three-electrode cell.

4. Results and discussions

The main steps for the development, optimization and characterisation of the high temperature NiCrBSi-TiB_2 vacuum furnace fused flame-sprayed coatings can be schematically seen in Figure 4.1.

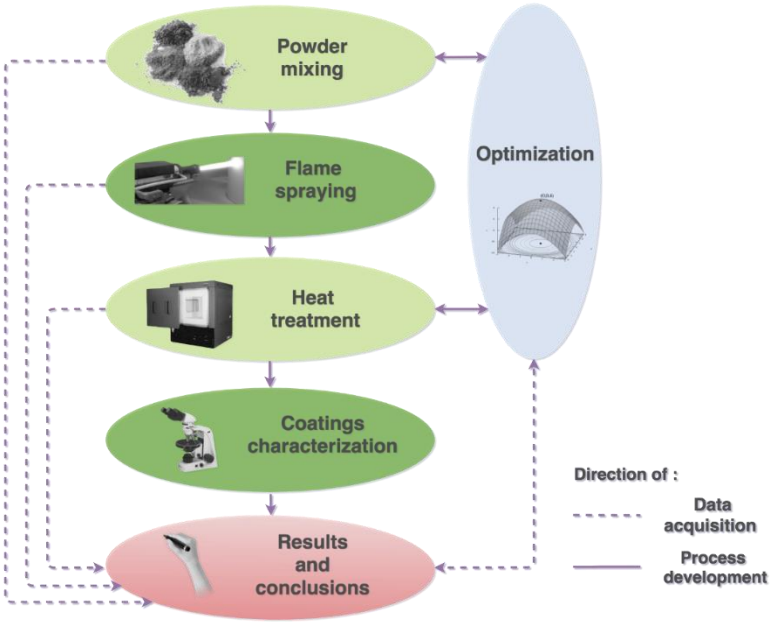

Figure 4.1 Schematic diagram of the experimental procedure

Materials

Substrate material

The importance of the substrate material is undisputable. The base material has to be perfectly adapted to the application for which it was chosen and the materials to be coated. It is important to select a substrate that is widely used in the industry. In this way, it is in a way assured that the developed coating can be used on a large industrial scale. In the current study, the structural steel S355JR was used as a substrate, a material widely used in the industry.

The most favourable substrate geometry for performing the scientific tests has been decided to be 50x20x15 mm. The machining of the samples has been done according to this specification. A degreasing has been first performed to obtain a substrate that complies with the Sa 3 class of cleanliness required by the EN ISO 8501 [5]. A grit blasting has been performed with chilled iron and a roughness between 70 µm and 100 µm has been obtained, as required by the American Navy Standard MS 2138 [6]. To protect the substrate from possible contaminations from the atmosphere, the grit-blasting has been performed in a separate room dedicated only to this procedure. The grit-blasting was the last procedure in the preparation of the substrate. Shortly after this step, the coating material was deposited.

Matrix material

Once deposited, the thermally-sprayed coating should be considered as an integral part of the product. In a thermally sprayed component, several materials have to be compatible with each other for the part to have a long life-cycle.

The Ni-based self-fluxing alloys are known for the good homogeneity of the coatings and their good wear resistance. For the present work, a NiCrBSi powder from the company LSN Diffusion commercialized under the N-330 name has been used. The chemical composition of the material can be seen in *Table 4.1*.

Table 4.1 The chemical composition of the NiCrBSi powder

	Ni (%)	*Cr (%)*	*B (%)*	*Si (%)*	*Fe (%)*	*C (%)*
NiCrBSi (N-330)	bal.	6	1	4	1.5	0.3

The manufacturer reported size of the water-atomized powder was -60 +100 µm. In *Figure 4.2* the SE micrograph demonstrates both the spheroid shape and the size of the material. Advantages like smaller energy input or uniform heating arise when using such powder production technologies.

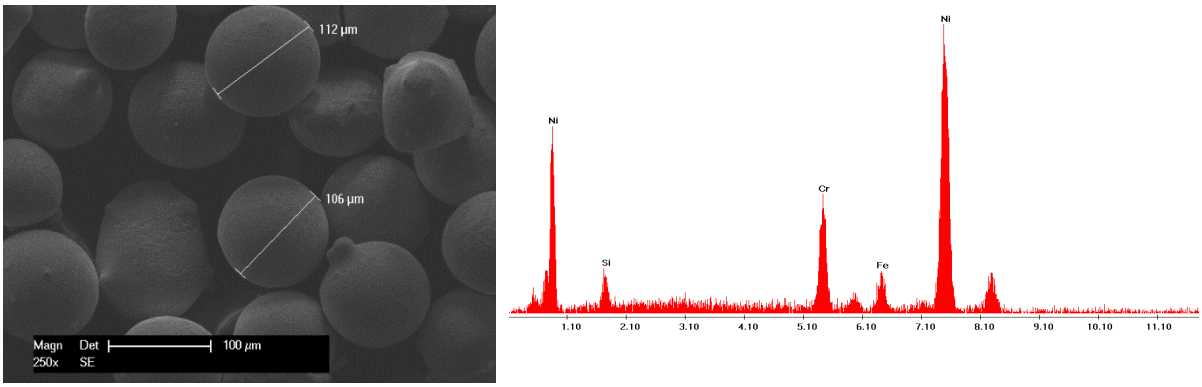

Figure 4.2 Micrographs presenting (left) the topography and (right) the EDX spectrum of the NiCrBSi powder

An EDX analysis of the NiCrBSi powder can be seen in *Figure 4.2*. The balance element Ni dominates the spectrum having the most intense peaks. After Ni, the carbide forming element Cr has the highest peak. Carbides are known to be hard compounds and to have a favourable effect on the wear resistance of thermally sprayed coatings. Si although finding itself in the chemical composition in a small quantity promotes, in combination with B, the deoxidation and the wettability of the coating during the heat treatment. Si tends to form phases with both Ni and Fe, influencing the structure of the matrix in the coating.

The melting range of the material is a very important aspect in the context of an industrial use. The whole deposition process is adjusted in function of the melting range of the powder, which was in this case determined using a thermogravimeter. In the thermogram presented in *Figure 4.3* the range of temperature that is relevant is between approximately 920°C and 1150°C. The melting range is starting at 1009°C, the material being completely melted at 1068°C. Therefore, this chemical composition of Ni-based powder will have to be deposited and heat-treated at a temperature of at least 1050°C. Si and B are lowering the melting temperature of the matrix material and stabilizing it at the same time [7]. Moreover, the addition of Si in the alloy is increasing the self-flux ability of the material.

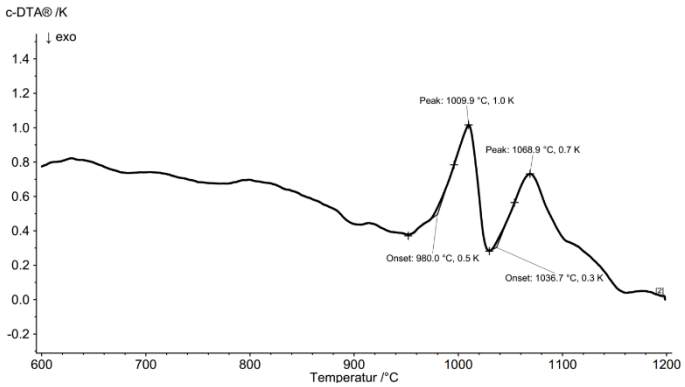

Figure 4.3 DTA curve of the NiCrBSi powder

Reinforcing material

TiB_2 is a relatively studied ceramic in the medical, thin film and aeronautic industries. The high hardness, good creep resistance, thermal conductivity and chemical stability are just some of the properties that make the compound attractive to use in the coating industry. The material can crystallize in an orthorhombic or hexagonal crystalline cell, both structures being an advantage for decreasing the wear rate of TiB_2 coatings. Another positive aspect in using

TiB_2 for the coating industry is that the majority of the properties do not change at room and elevated temperature [8,9].

The TiB_2 powder used for the current work was produced by the German company H.C. Starck. The chemical composition of the powder can be consulted in *Table 4.2*.

Table 4.2 Chemical composition of the TiB_2 powder

	B *min (%)*	*C* *max (%)*	*O* *max (%)*	*N* *max (%)*	*Fe* *max (%)*
TiB_2	min. 30	6	1	4	1.5

SEM micrographs of the compound can be seen in *Figure 4.4*. The particle size distribution of the TiB_2 varies between 3.5 µm and 8 µm. As it can be observed in *Figure 4.4*, the topography of the particle is irregular. On one hand, during the feeding and thermal spraying process, it can be an unfavourable aspect because it can easily create difficulties in the flowing of the material through the powder carrier system. On the other hand, the material being mixed with the spheroidized Ni-based matrix, it creates the possibility of a powerful hooking between the two powders, making possible a uniform flow in the feeding system.

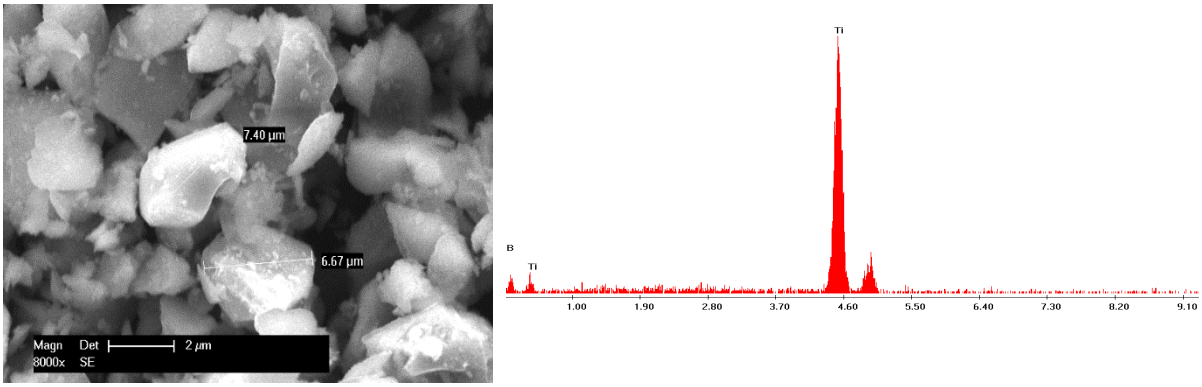

Figure 4.4 Micrographs presenting (left) the topography and (right) the EDX spectrum of the TiB_2 powder

The EDX spectrum from *Figure 4.4* confirms the chemical composition of the delivered powder. The powder manufacturer reported a powder size range of -3.5 +7 µm.

Powder mixing

The matrix and the reinforcement materials have been mixed in four different volumetric proportions using a screw conveyer. Several advantages of the powder mixing technology motivated the decision to use this technology for the present work. The screw conveyors inherently ensure that the NiCrBSi and TiB_2 powders are constantly mixed while, the combining of the materials through the rotating spiral eliminates the risk of segregation of the smaller reinforcing material. The cost-effectiveness of the method can as well be big advantage for powder analysis in industry.

Table 4.3 The four NiCrBSi-TiB_2 volumetric mixes considered for investigations

Designated name	*NTB5*	*NTB10*	*NTB15*	*NTB20*
NiCrBSi:TiB_2 vol. %	95:5	90:10	85:15	80:20

Comparing the topography of the NiCrBSi and TiB_2 material, it is easy to observe the size difference of the powders. When mixing materials with such a size dissimilarity,

maintaining the integrity and avoiding the degradation of the powders is as well a challenge during the process. It can be observed in *Figure 4.5* that, when using a screw conveyor, the two materials are carefully mixed in a way that makes the small TiB_2 attach as satellites of the much bigger in size NiCrBSi matrix.

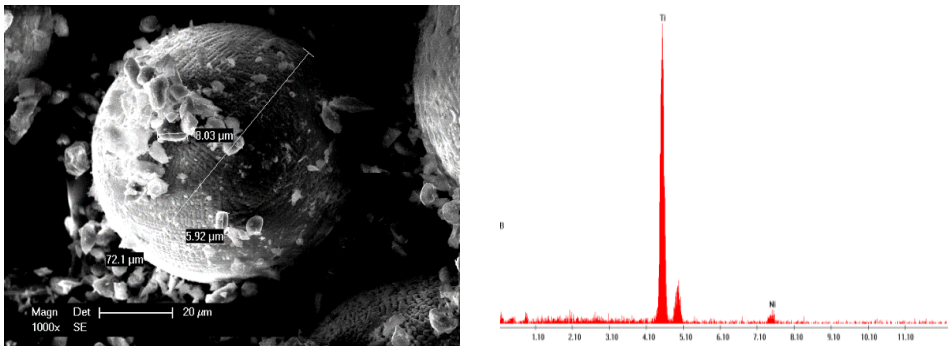

Figure 4.5 SE micrographs (left) of the mixed powders and EDX spectra (right) of the TiB_2 powder

Powder deposition

The material deposition process is an extremely important step to obtain the desired characteristics of the coating. The operating parameters have been attentively set according to the characteristics of both the depositing and the substrate material and they can be consulted in *Table 4.4.*

Table 4.4 The main operating conditions of the thermal spraying process

Parameters	*Materials/conditions/values*
Sprayed material	NiCrBSi – TiB_2
Substrate material	Structural steel
Surface roughening	
Surface roughening method	Grit blasting
Roughening material	Chilled iron grit
Surface roughness after roughening	min. 75 µm
Flame spraying gun producer	Metatherm
Flame generation	
Fuel gas	Acetylene (C_2H_2)
Secondary gas	Oxygen (O_2)
Flame stoichiometry C_2H_2:O_2	1:2
Substrate temperature	≈ 105°C
Spraying temperature	≈ 2850°C
Fusion temperature	≈ 1100°C
Particle velocity	100 m s^{-1}
Coating deposition	
Powder feed rate	2.5 kg h^{-1}
Stand-off distance	120 mm.
Propelling gas	Purified air
Relative gun motion	Translation over the samples

Before the actual deposition, the substrate has been brought to the cleanliness normed values of the EN ISO 8501 standard through decreasing and water and alcohol cleaning. The blasting was performed in a dedicated room to avoid the contamination of the substrate material.

Vacuum furnace optimization of the fusing process

Putting it simply, the Design of Experiments (DOE) is a method of gathering the maximum amount of information from samples arranged in a design space by using a minimum

amount of probes and invested energy. As each sample is time and resource consuming, it is legitimate to try to limit the needed effort. The response surface methodology (RSM) is an intuitive statistical approach to increase the quality by employing a cheaper step by step path where fewer experimental runs are required and a high statistical efficiency is reached.

For Ni-based self-fluxing alloys, the thermal post-treatment of the coating is highly important. The post-treatment and its results can largely influence the quality of the entire deposition. For this reason, the optimization process of the heat treatment parameters is strongly recommended. The flowchart of the followed steps of the optimization can be seen in *Figure 4.6.*

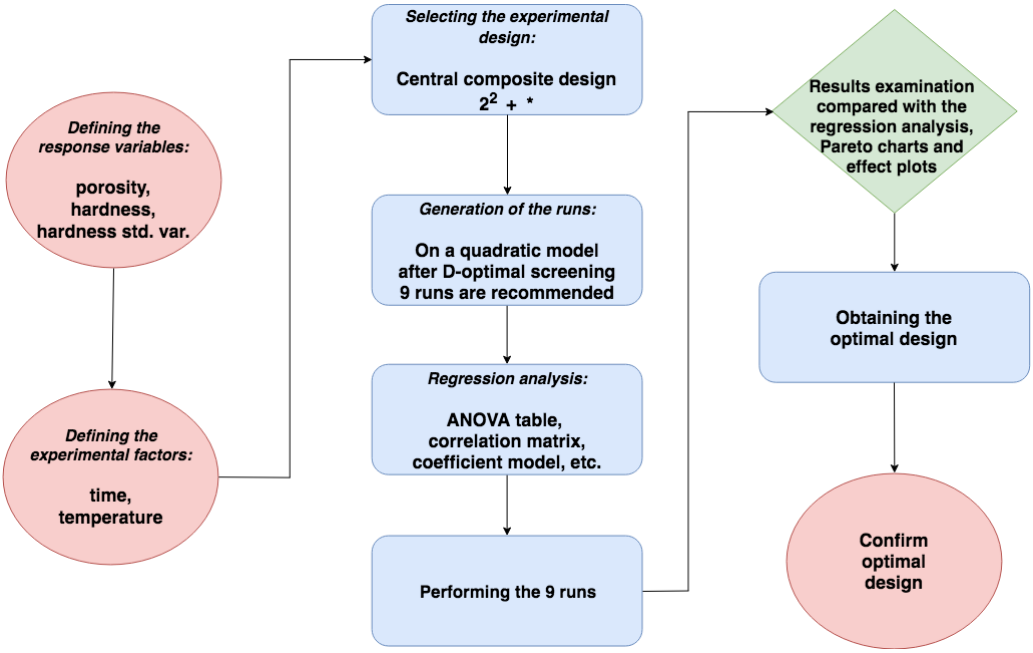

Figure 4.6 RSM flowchart procedure for the optimization of the vacuum heat treatment parameters

The response variables selected for the present work have been the porosity, the hardness and its standard deviation. These parameters have been extensively used as responses in the optimization of thermal spraying coatings [10–13].

The porosity is highly important when it comes to TS. The void content, shape and measurement is present in all the technologies and can vary extremely much. An interconnected porosity can be disastrous with regard to corrosion or wear. When it comes to the resistance or machinability of the coating, the porosity plays an important role as well. The microhardness and its standard deviation can give us other hints about the quality of the deposition. The resistance of the material to plastic deformations characterizes the level of strength of the intermolecular bonds. The ductility, the strength or the viscosity are just a few of the elements that depend on the hardness. The standard deviation of the microhardness is a parameter that gives an indication on the uniformity of the coating. Although by microindentation is very likely to hit several phases of the material and have different values, it is essential to measure the same value of the same phase in the whole coating. Considering the importance of these parameters, selecting the porosity, the hardness and the hardness deviation as responses of the design was an obvious choice.

The two followed process factors in this experimental design, time and temperature, are controllable and they can be regulated during the process in order to enhance the process quality. In consequence, A: Time has been set to take between 30 min. and 90 min., values chosen in accordance to peer reviewed literature [14–16], and B: Temperature has to be

maintained between 1020°C and 1110°C, based on the melting range of the matrix material determined by the termogravimetric measurements.

The central composite design 2^2 + star consists of several points, each of them being attributed a time and a temperature value. The design is a form of the 2^k CCD (*i.e.* Box-Wilson design) where *k* is given by the number of controllable factors. This design is considered advantageous as it consists of a relative small number of runs in comparison with other types of designs.

The mathematical equation $\hat{Y}$ of the of the statistical model is described as:

$$\hat{Y} = A_0 + A_0B_1 + A_2B_2 + A_3B_3 + A_{12}B_1B_2 + A_{13}B_1B_3 + A_{23}B_2B_3 + A_{11}B_1^2 + A_{11}B_2^2 + A_{11}B_3^2 \quad (4.1.)$$

where the experimental factors A (time) and B (temperature) are considered. Each factor of the equation is giving a combination of time-temperature values recommended for an experimental run. The results of the generated quadratic central composite design can be consulted in the *Table 4.5* and *Table 4.6*

Table 4.5 Results of the experimental program for the NTB5 and NTB10 batches

			NiCrBSi+5%TiB₂				*NiCrBSi+10%TiB₂*			
n	t (min)	T (°C)	$\bar{P}$ (%)	$\bar{H}$ (HV0.3)	σ	D [a]	$\bar{P}$ (%)	$\bar{H}$ (HV0.3)	σ	D [a]
1	30	1020	5.99	330	34	0.53	*3.44*	*346*	*48*	*0.71*
2	90	1020	*2.25*	*311*	*34*	*0.71*	3.8	318	78	0.53
3	30	1110	2.08	288	39	0.66	1.28	346	137	0
4	90	1110	1.3	277	42	0.66	1.02	302	89	0.52
5	28	1065	3.88	304	28	0.63	3.94	310	64	0.55
6	92	1065	2.83	352	80	0.59	9.6	366	117	0
7	60	1016	9.96	301	37	0.05	7.7	332	64	0.38
8	60	1114	3.9	315	47	0.61	8.03	289	47	0.25
9	60	1065	6.84	319	89	0.33	13.64	319	89	0

[a] *Desirability*

Table 4.6 Results of the experimental program for the NTB15 and NTB20 batches

			NiCrBSi+15%TiB₂				*NiCrBSi+20%TiB₂*			
n	t (min)	T (°C)	$\bar{P}$ (%)	$\bar{H}$ (HV0.3)	σ	D [a]	$\bar{P}$ (%)	$\bar{H}$ (HV0.3)	σ	D [a]
1	30	1020	5.28	344	52	0.51	4.88	337	51	0.58
2	90	1020	4.25	320	38	0.55	7.23	314	79	0.32
3	30	1110	3.23	344	45	0.63	*1.98*	*351*	*43*	*0.71*
4	90	1110	*1.12*	*321*	*37*	*0.82*	1.41	332	86	0.47
5	28	1065	7.23	320	59	0.35	3.87	344	79	0.51
6	92	1065	3.22	345	40	0.7	1.47	371	142	0
7	60	1016	14.2	325	24	0	5	318	39	0.57
8	60	1114	2	314	24	0.75	1.3	293	62	0.61
9	60	1065	3.46	337	52	0.65	3	335	67	0.58

[a] *Desirability*

The desirability *D* concept, developed by *Myers and Montgomery*, is a very popular and easy to visualize multiple response method in statistical optimization [17] . The idea behind the concept is that values of a particular process or product must be inside its defined limits. The approach assigns a score between 0 and 1 to the results of the responses.

The general form of the overall desirability equation with *t* runs takes the following form:

$$D = \left(d_1(Y_1)d_2(Y_2)\cdots d_k(Y_k)\right)^{1/t} \quad (4.2.)$$

Applying *Eq. (4.2.)* to the present case, the overall desirability function is:

$$D = \left(d_1(\bar{P})_1 d_2(\overline{H})_2 d_k(\sigma_k)\right)^{1/9} \tag{4.3.}$$

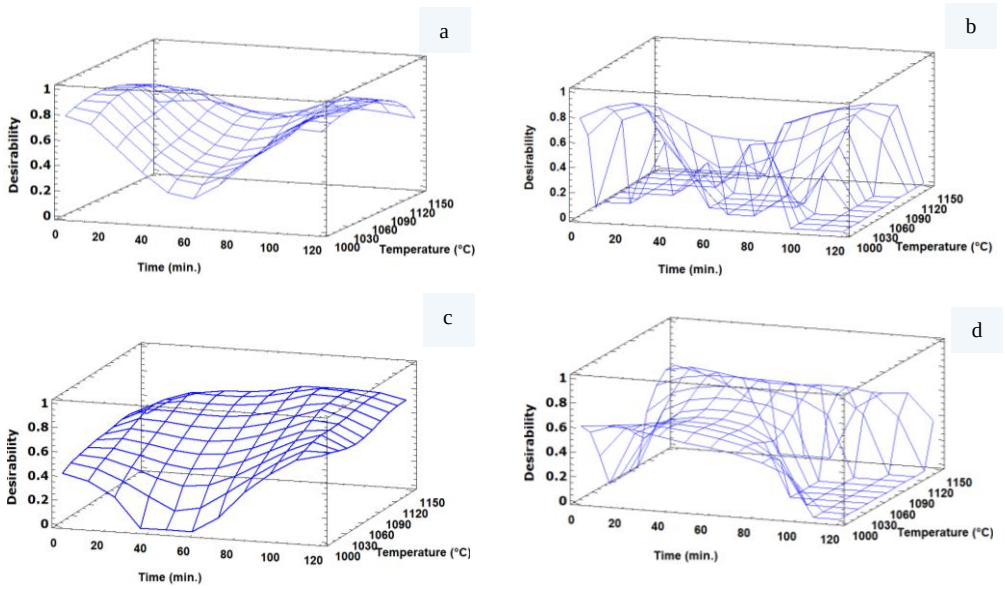

Table 4.7 Desirability plot of the (a) NTB5, (b) NTB10, (c) NTB15 and (d) NTB20 samples

As general remarks, it can be observed on one hand that at medium combination of the two variables a decrease is occurring in the plots. On the other hand, the highest peaks for all the plots are achieved at high temperatures and long holding times. Every plot of each batch reached a maximum desirability of over 0.7. Nevertheless, the only one crossing a 0.8 desirability point is the NTB15 batch.

Conclusively, it can be stated that in order to obtain optimum results for a vacuum heat-treated thermally sprayed NiCrBSi-TiB_2 sample, a combination of 85 vol.% matrix and 15 vol.% reinforcement should be used. The post-processing with a vacuum furnace at a holding time of 90 min. at a temperature of 1110°C should deliver the best results.

The heat-treatment program for the optimal parameters can be seen in *Figure 4.7.* The program shows a three-interval heating, the first being performed with 10°C min^{-1} up to 200°C. At this temperature the water and other possible compounds evaporate. The second heating ramp is performed with 10°C min^{-1} until 950°C. The temperature is under the melting range of the matrix material but high enough for a soaking of the material. A 10 min holding time should be enough for soaking as the samples are relatively small in size. A slow heating of 5°C min^{-1} has been performed followed by the holding of 90 min at 1110°C as determined by the optimization program. A slow cooling until 950°C has been performed to avoid introducing internal stresses. The last cooling ramp was at 10°C min^{-1} until the ambient temperature of 23°C was reached.

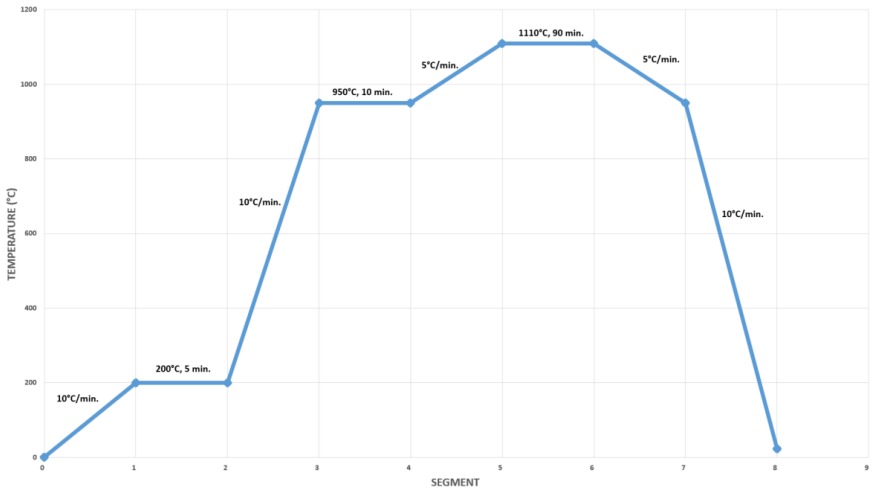

Figure 4.7 Optimized vacuum heat-treatment process parameters

The coatings with 15% TiB_2 and heat-treated with the *Figure 4.7* were the only reinforced coatings characterized and tested in the rest of the experimental program as these delivered the best results following the optimization process.

Characterization

Microstructure and phase composition

Figure 4.8 presents a detail of the NiCrBSi-TiB_2 sample in cross-section. The dark TiB_2 phases can be seen as heterogeneously distributed in the matrix. The non-homogeneous distribution is a consequence of the mixing process, the high melting point of the TiB_2 [18] and subsequently its ability to resist to solubility at the service temperature [19].

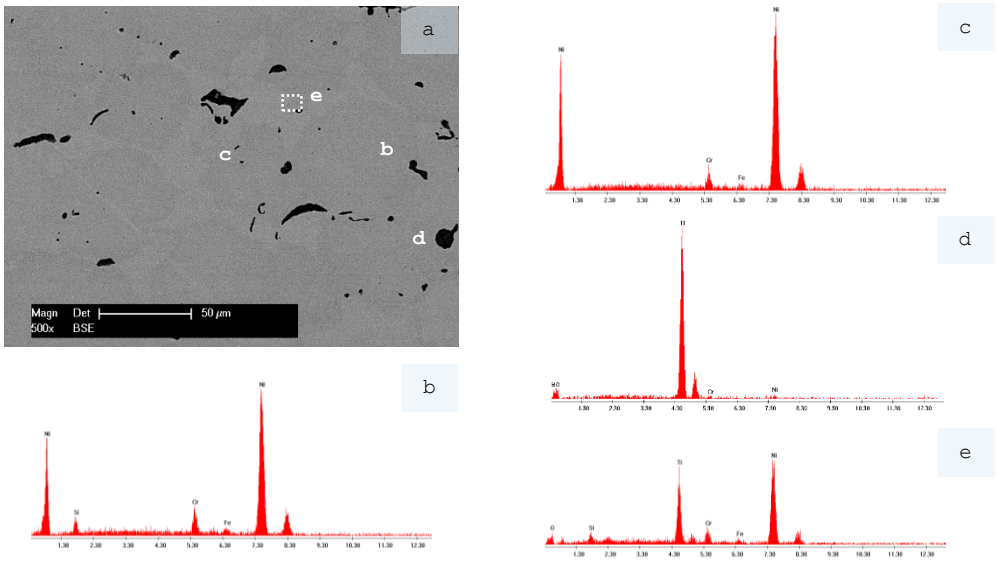

Figure 4.8 (a) SEM micrograph of NiCrBSi-TiB2 sample along with the corresponding (b),(c),(d),(e) EDX spectra

The EDX spot analyses from *Figure 4.8b, Figure 4.8c, Figure 4.8d and Figure 4.8e* correspond to different regions of the coating represented in *Figure 4.8a*. Corroborating the EDX spot analyses with the XRD spectra from *Figure 4.9*, the matrix noted with *b* in *Figure*

4.8a consists mainly of the tetragonal BNi_2 and the cubic γ-Ni. These eutectic structures are often detected as matrix in Ni-based thermal sprayed coatings research [20–23]. Another component in the matrix is the cubic σ-$Cr_3Ni_5Si_2$ phase. *Schuster et al*. [24] reported that the forming of the σ phase is favoured by the low Si content (4% in the present work). This structure can be consulted as well in the ternary Cr-Ni-Si diagram.

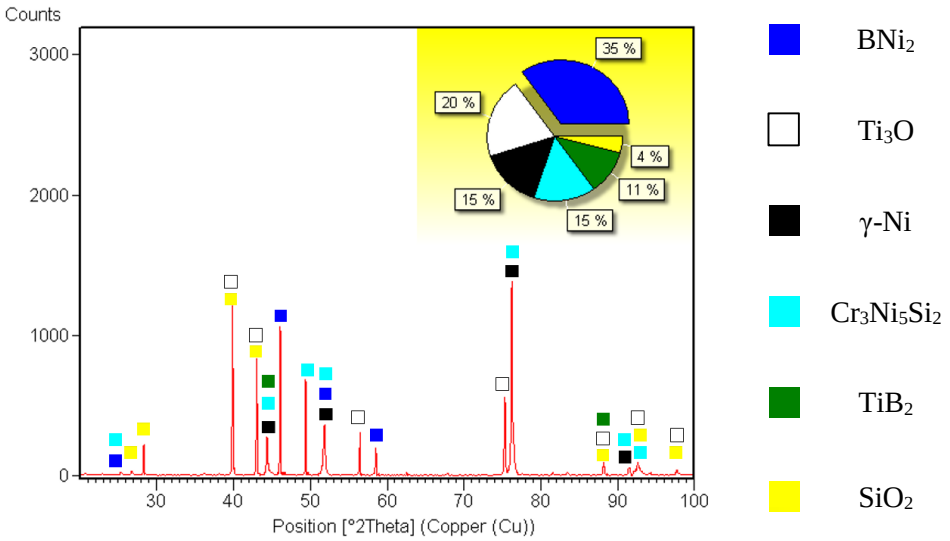

Figure 4.9 XRD diffractogram of the NiCrBSi-TiB_2 vacuum furnace heat-treated sample

A sign that the post-processing program was well defined is that Cr is detected in the σ-$Cr_3Ni_5Si_2$ phase and is not diluted in the Ni matrix forming minor constituents [25]. The rest γ-Ni/BNi_2 phase is found in the region *c* of *Figure 4.8a*. The area *d* on the SEM micrograph corresponds on one hand to the hard TiB_2 phase that is expected to aid the wear resistance of the coating [26,27] and on the other hand to the Ti_3O.

The operating pressure of the vacuum pump is 10^{-6} mbar and the elimination of the majority of the oxides and gases is successfully done. Nevertheless, Si and Ti both have a high susceptibility of forming oxides until an oxygen partial pressure of about 10^{-23} mbar [28] according to the Ellingham diagram. Therefore, the formation of SiO_2 and Ti_3O is inevitable.

Adhesion

The performance and the quality of a TS coating is dependent on the coating-substrate adhesion. A possible debonding would inevitably result in a collapse of the whole system. The bonding mechanisms in thermal spraying depend on the contact between the splats and between the splats and substrate.

By analysing the line-scan at the interface in *Figure 4.10*, an area between 125 µm and 175 µm can be observed where the content of Ni decreases and the one of Fe is increasing. It can be stated that in the approximately 50 µm region a metal-to-metal bonding is formed, one that should be much stronger than the typical mechanical interlocking found in thermal spraying.

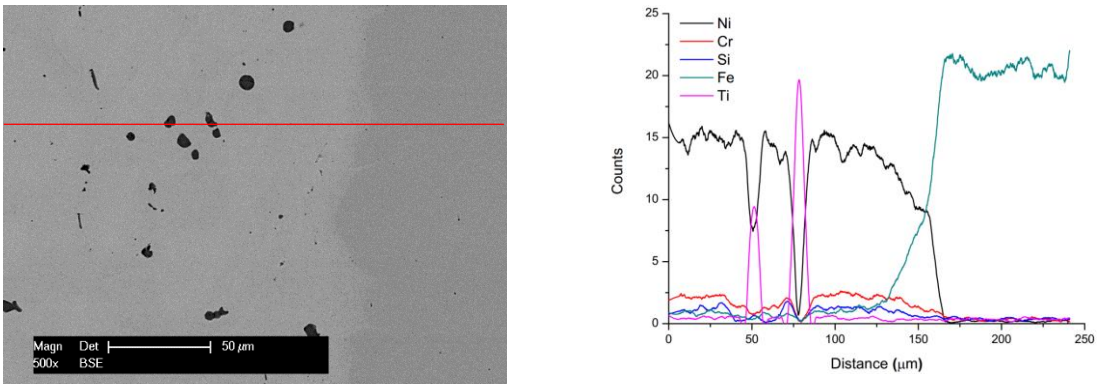

Figure 4.10 BSE micrograph of the interface and the corresponding line-scan graph

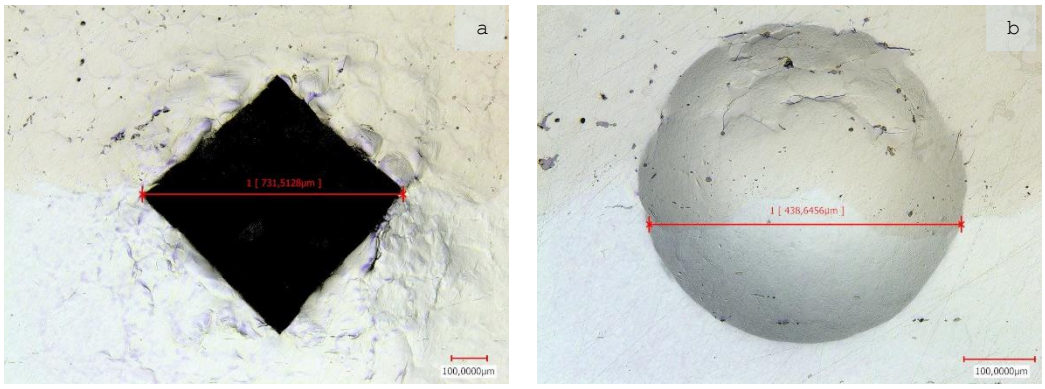

Figure 4.11 Micrographs showing the imprints of the a) Vickers and b) Brinell indentations

Several indentations have been performed until a load of 50 kgf on the HV scale and 62.5 kgf on the HBW scale was reached. Although large indentations have been obtained, no visible cracks could've been observed at the tips of the indenter. The results denote an excellent interface adhesion, low internal stresses and a high interfacial fracture toughness. The crack free area indicates also a good choice of a series of interdependent factors in the coating building like: the substrate material (roughness, cleanliness), the operating conditions or the feedstock morphology and particle size distribution.

Tribological behaviour

Several tools and determined values have been used and compared in order to perform a comprehensive analysis. Vacuum-remelted NiCrBSi coatings deposited with the same matrix material has been employed as comparison sample with the NiCrBSi-TiB_2 sample. The result analogy is extremely important as it can give an idea of how the developed coating is behaving in the same conditions as one that is already used in the industry.

The tribological behaviour was analysed with a pin-on-disk equipment. Prior to the tests, the samples have been grounded with a 100 grain size SiC paper. An analysis of a section of a wear track was performed by using 3D topographical maps acquired with the CSL microscope. By measuring the depth and width of the wear tracks in distinct spots it was possible to calculate the wear rate of the samples. *Figure 4.12* shows a clear difference between the profiles of the four evaluated samples. The upper samples tested against a 100Cr6 ball exhibit a wider track than the ones evaluated against the WC-Co ball. The steel counterpart being a much softer material than the carbide, it will degrade faster during the test and the amount of dislocated

material will be higher. The effect of the bigger dislocated material can be also seen in the diameter of the spherical caps. On the tests realized on the NiCrBSi-TiB_2 samples but most notably in *Figure 4.12d,* small asperities can be seen on the wear track. This is realized by the pull-out effect due to the adhesion between the sample and the static partner.

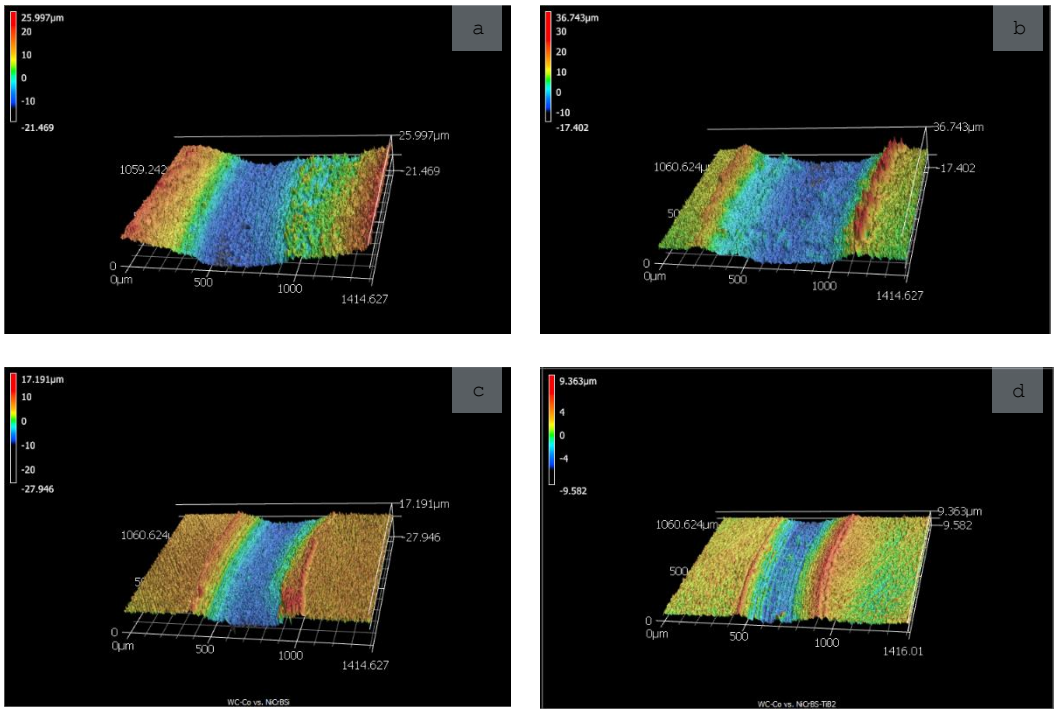

Figure 4.12 Wear track profile of (a) NiCrBSi and (b) NiCrBSi-TiB_2 vs. 100Cr6 and (c) NiCrBSi and (d) NiCrBSi-TiB_2 vs. WC-Co

SEM micrographs and EDX spectra of the NiCrBSi-TiB_2 coating against the 100Cr6 and WC-Co ball can be seen in *Figure 4.13a* and *Figure 4.13b*. As expected, in the SE representations, different phenomena can be seen happening for the experiments with the two different static partners. The higher wear rate of the NiCrBSi-TiB_2 coating against the 100Cr6 ball can be attributed to layers transferred from the counterpart to the coating. As the EDX analysis confirms, parts of the steel ball smeared on the surface of the NiCrBSi coating forming a transfer layer between the surfaces in contact. When the coating is exposed to a harder static partner regions of spalling can be observed. These areas are encountered just when tested against a very resistant WC-Co counterpart showing that the coating exhibits a good inter-splat bonding. No microcracks can be seen on the surface, which shows that a good cohesion between the different phases has been realized through the post-treatment. As general remarks, no delamination or brittle fracture can be seen on the worn surfaces due to the low internal stresses found in the coating. The wear tracks of the NiCrBSi-TiB_2 coatings are fairly smooth after the test showing a good wear resistance against both steel and carbide counterparts.

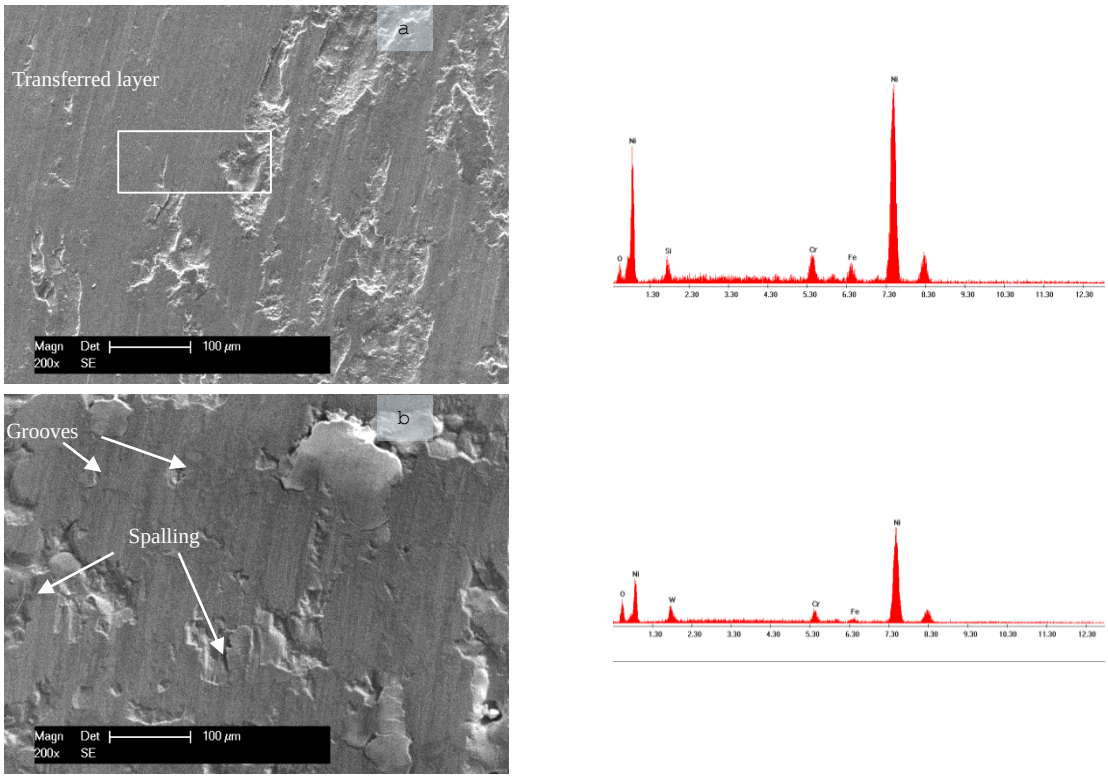

Figure 4.13 SE micrograph of the wear track of NiCrBSi-TiB_2 sample vs. a) 100Cr6 and b) WC-Co counterpart and their corresponding EDX spectra

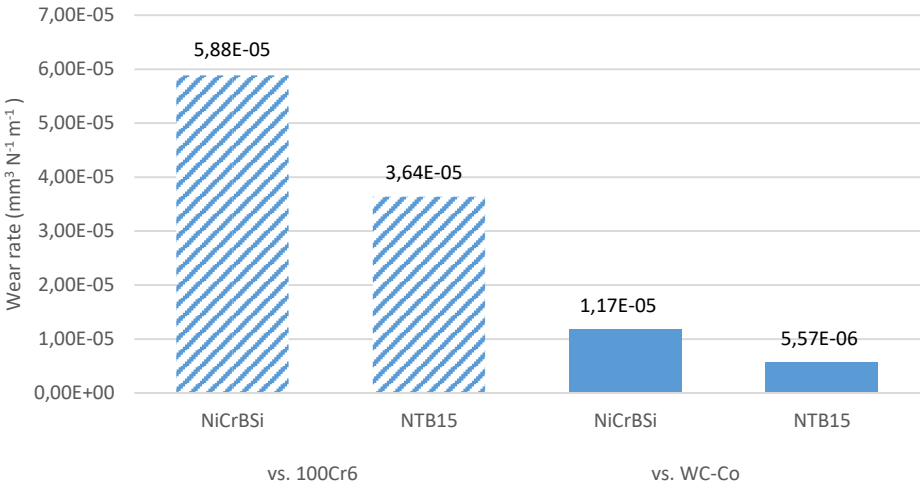

Figure 4.14 Wear rate of the NiCrBSi and NiCrBSi-TiB_2 coating

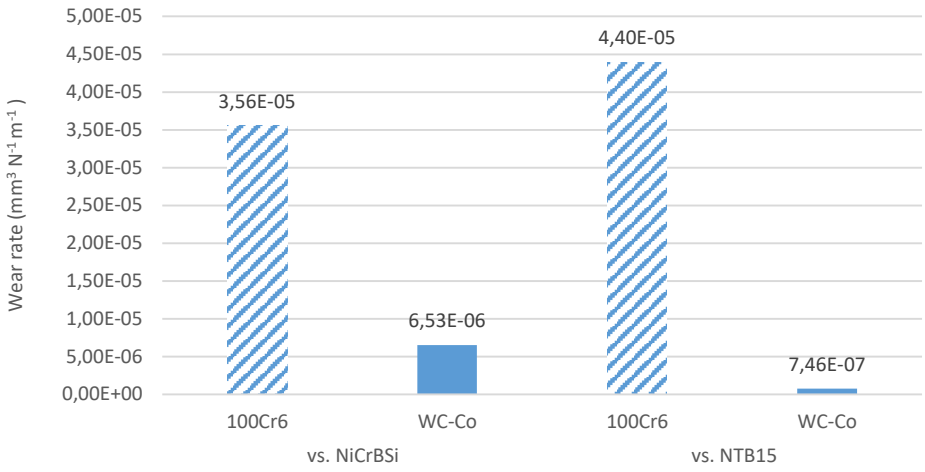

Figure 4.15 Wear rate of the 100Cr6 and WC-Co counterpart

When looking at the wear rates of the coatings, the NiCrBSi-TiB_2 showed both times a lower value than the NiCrBSi. The superiority of the coating is a result of the combination of factors such as the phase composition, a properly chosen furnace program and the used reinforcement, all of them leading to a resistance against the destructive test. Regarding the wear of the counterpart, the steel ball against the NiCrBSi-TiB_2 ended up with a bigger worn volume while in the case of the WC-Co ball a higher wear rate of the static partner could be observed when tested against the NiCrBSi coating.

Corrosion behaviour

Showing good corrosive behaviour, the self-fluxing Ni-based coatings can represent a good solution when exposed to seawater. The corrosion behaviour of the NiCrBSi-based coatings was assessed in 3.5% NaCl solution (pH~7), at room temperature, using a three electrode-cell configuration, applying qvasi stationary conditions (scan rate 0.16 $mV \cdot s^{-1}$). A SCE was defined as reference and a Pt disk as counter electrode.

Typical potentiodynamic polarization curves for the investigated samples in 3.5 wt.% NaCl solution can be seen in *Figure 4.16* as *i-E* representation and in *Figure 4.17* as log *i-E* representation.

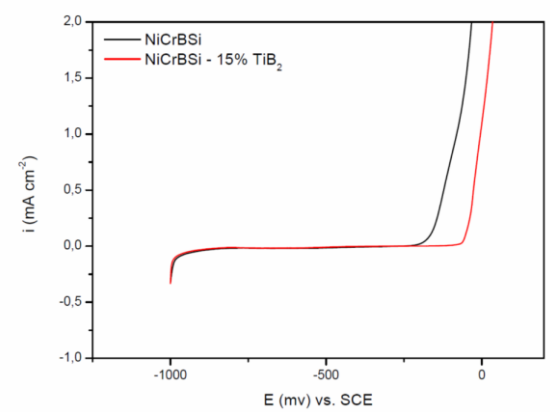

Figure 4.16 Linear plot of the polarization behaviour of NiCrBSi and NiCrBSi-TiB_2 in 3.5% NaCl

The semi-log plot of the polarization of the two coatings in 3.5% NaCl from *Figure 4.17* can deliver plenty of information regarding the behaviour of the samples in a seawater environment. Difference in both corrosions current and potential can be easily observed.

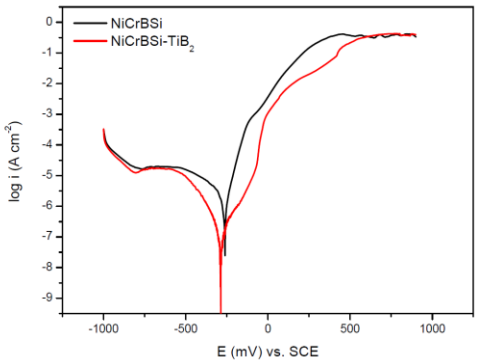

Figure 4.17 Semi-log plot of the polarization behaviour of NiCrBSi and NiCrBSi-TiB_2 in 3.5% NaCl

The solid metals corrode only at the surface of the parts while for thermal sprayed coatings, the corrosion can easily happen in the inner part of the coating due to several reasons (*e.g.* porosity). The dense structure of the NiCrBSi-TiB_2 sample exhibits a lower corrosion current (i_{corr}=0.7·10^{-7} mA cm^{-2}) in comparison with the reference NiCrBSi coating (i_{corr}=10·10^{-7} mA cm^{-2}), resulting in a superior corrosion resistance of the TiB_2 containing coating.

Table 4.15 Corrosion potential and corrosion current density values in 3.5% NaCl

Sample	E_{corr} *(mV) vs. SCE*	$E_{b.d.}$ *(mV) vs. SCE*	i_{corr} *(mA cm^{-2})*
NiCrBSi	-260	-240	10·10^{-7}
NiCrBSi – TiB_2	-290	-60	0.7·10^{-7}

Anodic metal passivation generally arises at a so-called passivation potential, in the anodic branch of the polarisation curve, and over this value, the anodic current for metal dissolution considerably decreases. This aspect indicates that the metallic passivity is produced by the generation of an oxide film on the metal surface, called usually passive film, which is extremely thin and protects the coating from a further oxidation. For most of the metal alloys, the passive film is less than several nanometres in thickness in the stable potential region. Depending on the Cr amount from the chemical composition, these alloys might exhibit a certain degree of passivation. The alloys which contain more than 12% Cr are able to form a stable passivation layer. The stability of the formed passive layer in a chlorine solution can be determined by means of such electrochemical polarisation tests.

For applications in which the present coating is employed, the corrosion E_{corr} and breakdown $E_{b.d}$ potential are important notions to follow. Corrosion experts consider that materials exhibiting higher values of $E_{b.d.}$ (defined as the potential at which the passive film is breaking) are more resistant to pitting corrosion. When comparing the two potentials, for the non-alloyed coating the values are very close, while for the TiB_2 a difference of about 200 mV can be noticed. Considering the above mentioned aspects, on may declare that the TiB_2 containing coating exhibits a better pitting corrosion resistance in comparison with the reference NiCrBSi coating.

Looking at the top view and cross-sectioned view of the corroded sample in *Figure 4.18* and *Figure 4.19*, it can be seen that the TiB_2 remain skeletal on the surface and do not dissolve in comparison to the Ni-based matrix and possibly act as an internal physical barrier to the corrosion propagation. The EDX spectra corresponding to the micrograph confirm the presence of Si, Ti, Ni and O_2. Therefore, it can be supposed that the Ti_3O phase, also identified through the XRD analysis, can act in this way as passivation compound, hence the over 200 mV E_{corr}-$E_{b.d.}$ difference and better behaviour of the composite coating on the anodic region of the polarisation curves.

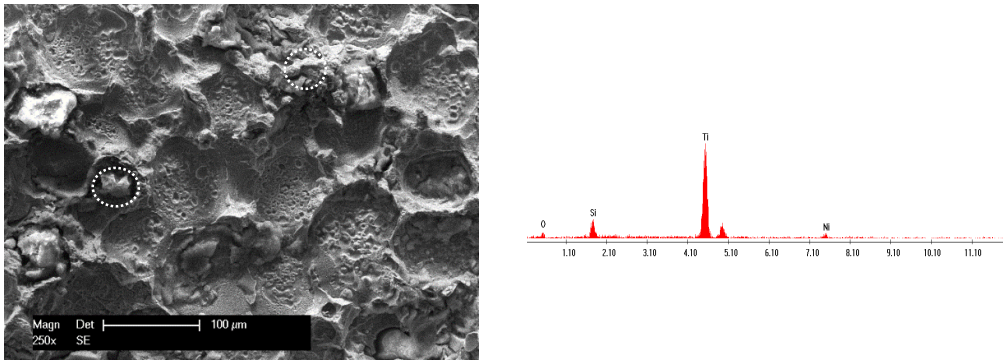

Figure 4.18 Top-view SE micrograph of the 3.5% NaCl NiCrBSi-TiB_2 corroded sample

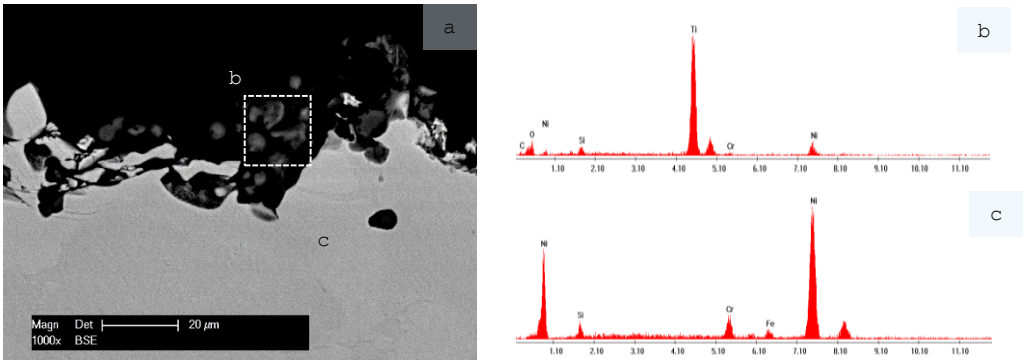

Figure 4.19 BSE cross-section micrograph and corresponding EDX spectra after electrochemical corrosion tests

In conclusion, the addition of corrosion resistance ceramic TiB_2 particles into the NiCrBSi matrix will reduce the degree of corrosion attack and consequently enhances the resistance of the coatings in chlorine containing environment.

5. Personal contributions

The personal contributions of the present study may be regarded as following:

- Reinforced NiCrBSi-TiB_2 mechanically mixed powder in different volumetric proportions were successfully thermally sprayed on a structural steel substrate in order characterize and investigate the behaviour of the coating against various mechanical and degradation tests
- Acknowledging the importance of the post-processing of self-fluxing coatings, a statistical approach was used to optimize the holding time and temperature during the vacuum furnace heat treatment and to select the best proportions among the samples with different matrix-reinforcement volumetric concentration in a close correlation with thermogravimetrical measurements
- A comprehensive characterisation using different methods was used to investigate the porosity, chemical composition, phase distribution and interface region of the optimized NiCrBSi-TiB_2 coating
- The tribological and corrosion behaviour of the reinforced coating was analysed in comparison with a conventional NiCrBSi alloy as reference

6. References

[1] Sagar A. A review on thermal spray coating processes. International Journal of Current Trends in Engineering & Research 2016;2:556–63.

[2] Hermanek FJ. Thermal spraying: what it was and what it has become. International Journal of Powder Metallurgy 2002;38:35–44.

[3] Vardelle A, Moreau C, Akedo J, Ashrafizadeh H, Berndt CC, Berghaus JO, et al. The 2016 Thermal Spray Roadmap. Journal of Thermal Spray Technology 2016;25:1376–440. doi:10.1007/s11666-016-0473-x.

[4] Koch GH, Michiel PH, Thompson Neil. G., Virmani YP, Payer JH. Corrosion Costs and Preventive Strategies in the United States. Houston, US: NACE International; n.d.

[5] EN ISO 8501: Preparation of steel substrates before application of paints and related products - Visual assessment of surface cleanliness - Part 1: Rust grades and preparation of uncoated steel substrated and of streel substreates after overall removal of previous coatings 2008.

[6] MS 2138-A: Metal sprayed coatings for corrosion protection aboard naval ships (Metric) 1992.

[7] Salimijazi HR, Golozar MA, M.R. K. Effects of remelting processes on porosity of NiCrBSi flame sprayed coatings. Surface Engineering 2016;32:238–43. doi:10.1179/1743294415Y.0000000107.

[8] Basu B, Raju GB, Suri AK. Processing and properties of monolithic TiB2 based materials. International Materials Reviews 2006;51:352–74. doi:10.1179/174328006X102529.

[9] Munro RG. Material Properties of Titanium Diboride. Journal of Research of the National Institute of Standards and Technology 2000;105:709–20. doi:10.6028/jres.105.057.

[10] Pierlot C, Pawlowski L, Bigan M, Chagnon P. Design of experiments in thermal spraying: A review. Surface and Coatings Technology 2008;202:4483–90. doi:10.1016/j.surfcoat.2008.04.031.

[11] Lih W-C, Yang SH, Su CY, Huang SC, Hsu IC, Leu MS. Effects of process parameters on molten particle speed and surface temperature and the properties of HVOF CrC/NiCr coatings. Surface and Coatings Technology 2000;133–134:54–60. doi:10.1016/S0257-8972(00)00873-2.

[12] Bertrand G, Bertrand P, Roy P, Rio C, Mevrel R. Low conductivity plasma sprayed thermal barrier coating using hollow psz spheres: Correlation between thermophysical properties and microstructure. Surface and Coatings Technology 2008;202:1994–2001. doi:10.1016/j.surfcoat.2007.08.042.

[13] Jaworski R, Pawlowski L, Roudet F, Kozerski S, Petit F. Characterization of mechanical properties of suspension plasma sprayed TiO2 coatings using scratch test. Surface and Coatings Technology 2008;202:2644–53. doi:10.1016/j.surfcoat.2007.09.044.

[14] Stoica V, Ahmed R, Itsukaichi T. Influence of heat-treatment on the sliding wear of thermal spray cermet coatings. Surface and Coatings Technology 2005;199:7–21. doi:10.1016/j.surfcoat.2005.03.026.

[15] Mahmud TB, Farrokhzad MA, Khan TI. Effect of Heat Treatment on Wear Performance of Nanostructured WC-Ni/Cr HVOF Sprayed Coatings. Tribology Online 2017;12:18–28. doi:10.2474/trol.12.18.

[16] Makarov AV, Soboleva NN, Gibzun MS, Malygina IYu, Korobov YuS. Increasing the resistance of a NiCrBSi coating to heat wear by means of combined laser heat treatment. AIP Conference Proceedings 2018;2053:030037. doi:10.1063/1.5084398.

[17] Myers RH, Montgomery DC, Anderson-Cook CM. Response Surface Methodology: Process and Product Optimization Using Designed Experiments. 3rd ed. US: John Wiley & Sons, Ltd; 2009.

[18] Wu YS, Qiu WQ, Yu HY, Zhong XC, Liu ZW, Zeng DC, et al. Cycle oxidation behavior of nanostructured Ni60TiB2 composite coating sprayed by HVOF technique. Applied Surface Science 2011;257:10224–32. doi:10.1016/j.apsusc.2011.07.026.

[19] Zhu HB, Li H, Li ZX. Plasma sprayed TiB2–Ni cermet coatings: Effect of feedstock characteristics on the microstructure and tribological performance. Surface and Coatings Technology 2013;235:620–7. doi:10.1016/j.surfcoat.2013.08.040.

[20] Mrdak MR. Microstructure and mechanical properties of nickel-chrome-bor-silicon layers produced by the atmospheric plasma spray process. Vojnotehnicki Glasnik 2012:183–200.

[21] González R, García MA, Peñuelas I, Cadenas M, Fernández Ma del R, Battez AH, et al. Microstructural study of NiCrBSi coatings obtained by different processes. Wear 2007;263:619–24. doi:10.1016/j.wear.2007.01.094.

[22] Singh S, Kaur M. Solid particle erosion behaviour of NiCrFeSiBC/Cr3C2 composite coatings – Part II. Surface Engineering 2016;32:475–89. doi:10.1179/1743294414Y.0000000419.

[23] Karagoz M, Islak S, Buytoz S, Kurt B. Microstructural Characteristics of High Velocity Oxygen Fuel (HVOF) Sprayed NiCrBSi-SiC Composite Coating on a Low Alloy Steel, Elazig, Turkey: 2011, p. 13–21.

[24] Schuster JC, Du Y. Experimental investigation and thermodynamic modeling of the Cr-Ni-Si system. Metallurgical and Materials Transactions A 2000;31:1795–803. doi:10.1007/s11661-006-0248-y.

[25] Sampath S, Neiser RA, Herman H, Kirkland JP, Elam WT. A structural investigation of a plasma sprayed Ni-Cr based alloy coating. Journal of Materials Research 1993;8:78–86. doi:10.1017/S0884291400120369.

[26] Barsoum MW, El-Raghy T, Rawn CJ, Porter WD, Wang H, Payzant EA, et al. Thermal properties of Ti3SiC2. Journal of Physics and Chemistry of Solids 1999;60:429–39. doi:10.1016/S0022-3697(98)00313-8.

[27] Duarte LI, Klotz UE, Leinenbach C, Palm M, Stein F, Löffler JF. Experimental study of the Fe–Ni–Ti system. Intermetallics 2010;18:374–84. doi:10.1016/j.intermet.2009.08.008.

[28] Atkins P, de Paula J. Physical Chemistry: Thermodynamics, Structure, and Change. 10th ed. W.H. Freeman and Company; 2014.